Research Article

Received: 27 July 2023 Revised: 27 February 2024 Accepted article published: 22 March 2024 Published online in Wiley Online Library: 16 April 2024

(wileyonlinelibrary.com) DOI 10.1002/ps.8102

Discovery of novel acrylopimaric acid triazole derivatives as promising antifungal agents

Xu Han,[a] Renle Xu,[a] Shihao Gu,[a] Yue Kong,[a] Yuhang Lou,[a] Yanqing Gao,[b*] Shibin Shang,[c] Zhanqian Song,[c] Jie Song[d] and Jian Li[a*]

Abstract

BACKGROUND: To further develop potential natural fungicides, two series of new acrylopimaric acid triazole derivatives were synthesized, and their antifungal activities were tested and evaluated.

RESULTS: *In vitro* antifungal activity results indicated that compound 5m **exhibited significant inhibitory activity against *Rhizoctonia solani* with an half maximal effective concentration (EC_{50}) value of 1.528 mg/L. Its antifungal effect was comparable to that of the commercially available fungicide fluconazole, epoxiconazole and propiconazole (EC_{50} values of 1.441, 0.815 and 1.173 mg/L). Subsequently, *in vivo* studies were conducted on compound** 5m**, which revealed its significant protective and curative effects against *R. solani*. In addition, physiological and biochemical studies showed that compound** 5m **could disrupt the morphology and ultrastructure of *R. solani* mycelium, increase cell membrane permeability, inhibit ergosterol synthesis, and enhance the activity of defense enzymes in rice plants. Three-dimensional quantitative structure–activity relationship (3D-QSAR) studies revealed that the molecular structure significantly influenced the binding of compound** 5m **to the receptor, thereby enhancing its antifungal activity.**

CONCLUSION: Compound 5m **exhibits excellent antifungal activity against *R. solani*, making it a promising candidate fungicide for the prevention and control of *R. solani*.**
© 2024 Society of Chemical Industry.

Supporting information may be found in the online version of this article.

Keywords: rosin; triazole; *Rhizoctonia solani*; antifungal activity; action mechanism

1 INTRODUCTION

Sheath blight of *Oryza sativa* (rice), caused by *Rhizoctonia solani*, is one of the major diseases in global rice production.[1] *Rhizoctonia solani* occurs throughout the entire growth period of rice and primarily affects the leaf sheaths and leaves. This poses challenges for its prevention and control, significantly impacting the high yield and stable production of rice.[2–5] In China, *R. solani* affects approximately 1.5 to 2 million hectares of rice, causing an annual yield loss of 6 million metric tons of rice grains.[6] Currently, due to the lack of resistant rice varieties, control measures for *R. solani* still rely on the use of chemical fungicides.[7–9] However, the intensive and continuous use of the same fungicides has not effectively controlled *R. solani*, which has increased the risk of pathogen resistance development. Therefore, the development of new green fungicides for the prevention and control of *R. solani* is highly necessary.

Plant-derived natural compounds have high selectivity in controlling pathogens, with minimal adverse effects on the environment. Compared to synthetic agricultural chemicals, they are considered ideal lead compounds for the development of natural product-based pesticides. In addition, studies have shown that natural products found in most plants can disrupt the original structure of cells and impact the synthesis of substances within them.[10–12] Therefore, the substances in plant extracts that are effective against *R. solani* can serve as alternatives to chemical fungicides, meeting the urgent need for developing green pesticides.

Rosin is a natural and renewable resource derived from pine. Its unique structure and excellent biological activity have made it widely utilized in the production of agricultural chemicals.[13–15] However, rosin is prone to oxidative degradation, which often necessitates modifications and optimizations of its molecular structure.[13]

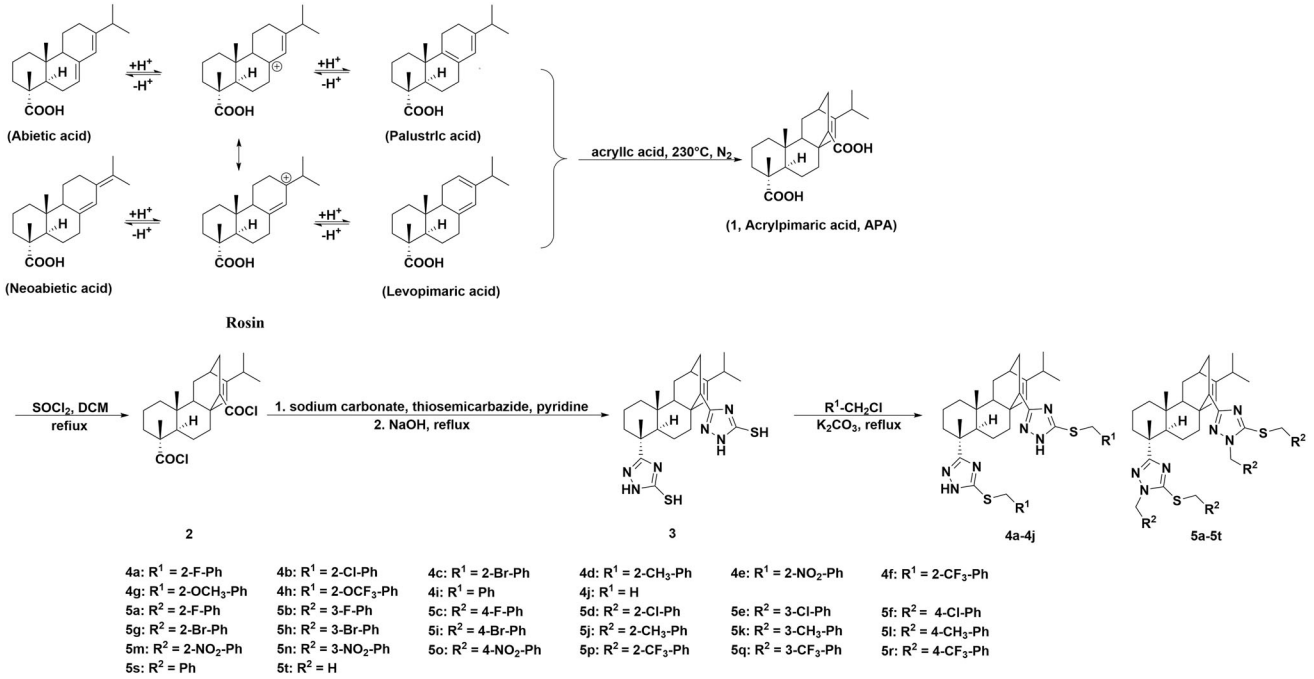
* *Correspondence to: Y Gao, College of Plant Protection and College of Forestry, Northwest A&F University, Yangling, Shaanxi 712100, P. R. China, E-mail: gaoyanqinggc@nwsuaf.edu.cn; or J Li, Jiangsu Province Key Laboratory of Biomass Energy and Materials, College of Forestry, Northwest A&F University, Yangling, Shaanxi 712100, P. R. China. E-mail: ericlee99@nwsuaf.edu.cn*

a *Jiangsu Province Key Laboratory of Biomass Energy and Materials, College of Forestry, Northwest A&F University, Yangling, P. R. China*

b *College of Plant Protection, Northwest A&F University, Yangling, P. R. China*

c *Institute of Chemical Industry of Forest Products, Chinese Academy of Forestry, Nanjing, P. R. China*

d *Department of Chemistry and Biochemistry, University of Michigan-Flint, Flint, MI, USA*



Scheme 1. Synthetic routes of compounds **4a**–**4j** and **5a**–**5t**

Triazoles are an important class of heterocyclic compounds in active compound modification and design. They can interact with various receptors and enzymes through hydrogen bonding, van der Waals forces, and hydrophobic interactions, among other mechanisms.[16] Therefore, they exhibit a wide range of biological and pharmacological activities.[17–19] In addition, certain active groups can be introduced through substructure linkage to the 1,2,4-triazole heterocyclic structure to enhance their biological activity. This modification often results in improved antifungal activity compared to the original structural molecule.[20]

In this study, two series of rosin-based triazole derivatives containing benzylamino and benzylthio groups were designed and synthesized. The synthesized compounds were subjected to *in vitro* antifungal activity testing against various fungi, including *Colletotrichum orbiculare*, *Fusarium graminearum*, *Botrytis cinerea*, *Sclerotinia sclerotiorum*, *Magnaporthe oryzae*, and *R. solani*. To further evaluate the potential of these derivatives as agricultural fungicides, *in vivo* experiments were conducted on *R. solani*. Subsequently, the morphology and ultrastructure of the mycelium were observed, cell membrane permeability was measured, and changes in the ergosterol content and defense enzyme levels [superoxide dismutase (SOD), catalase (CAT), phenylalanine ammonia-lyase (PAL), and polyphenol oxidase (PPO)] were assessed. These experiments provided initial insights into the antifungal mechanisms of rosin-based fungicides.

2 MATERIALS AND METHODS

2.1 Synthetic procedures for acrylopimaric acid triazole (intermediate 3) and acrylopimaric acid triazole derivatives (4a–4j and 5a–5t)

According to a previously reported method, acrylopimaric acid (**1**) and acrylopimaric acid chloride (**2**) were prepared.[21] Pyridine, sodium carbonate, and thiosemicarbazide were mixed and stirred until dissolved. Then, acrylopimaric acid chloride was added dropwise to the mixture diluted with pyridine. The reaction was carried out at 25 °C, and after 2–3 h, a large amount of distilled water was added, resulting in the formation of a solid precipitate. The solid was dried and mixed with a 5% sodium hydroxide solution. The mixture was refluxed for 4 h, and then the pH was adjusted to between pH 5 and pH 7 with acetic acid, leading to the formation of another solid precipitate. The precipitate was collected by filtration, dried, and purified by column chromatography to obtain the acrylopimaric acid triazole. Finally, acrylopimaric acid triazole, benzyl chloride, and potassium carbonate were dissolved in ethanol, heated, and refluxed for 4 h. The product was separated by column chromatography to obtain the acrylopimaric acid triazole derivatives (Scheme 1).

2.2 Biological assays

Biological assays were used to preliminarily determine the antifungal activity mechanisms of *R. solani*. The specific assay contents included *in vitro* and *in vivo* antifungal activity assays, observation of mycelial morphology and ultrastructure, assessment of cell membrane permeability, measurement of reactive oxygen species (ROS), nuclear morphology, and mitochondrial membrane potential, determination of ergosterol in mycelial cells, and measurement of changes in defense enzyme content in plant leaves. The specific experimental methods are provided in the Supporting Information Methods S1.

2.3 Three-dimensional quantitative structure–activity relationship (3D-QSAR) analysis

The molecular structure of the target compound was constructed using SYBYL-X 2.1 software for three-dimensional quantitative structure–activity relationship (3D-QSAR) analysis. The molecular energy was minimized using the Tripos force field and Gasteiger–Hackel charges. The biological activity of compounds was associated with their structural features using partial least

 © 2024 Society of Chemical Industry.

Table 1. Antifungal activities of rosin-based triazole derivatives (**4a**–**4j** and **5a**–**5t**) against *Rhizoctonia solani*

Compound	EC_{50}	$y = a + bx$	R^2	95% CL (mg/L)
4a	1088.754	$y = -3.32 + 1.07x$	0.967	237.485–101 457.653
4b	1665.504	$y = -3.32 + 1.01x$	0.963	286.904–610 416.873
4c	1273.095	$y = -3.62 + 1.22x$	0.945	257.768–184 536.278
4d	697.597	$y = -3.55 + 1.26x$	0.984	194.334–20 492.847
4e	613.559	$y = -3.37 + 1.21x$	0.978	180.094–14 184.661
4f	800.645	$y = -3.23 + 1.20x$	0.878	198.880–38 307.329
4g	849.179	$y = -3.38 + 1.23x$	0.936	209.032–42 628.083
4h	529.804	$y = -3.63 + 1.42x$	0.919	167.990–9007.277
4i	1437.619	$y = -3.41 + 1.08x$	0.959	270.130–312 343.809
4j	786.764	$y = -3.36 + 1.21x$	0.958	202.034–32 461.665
5a	2.059	$y = -0.34 + 1.12x$	0.973	1.023–3.177
5b	2.384	$y = -0.44 + 1.17x$	0.990	1.278–3.566
5c	2.070	$y = -0.37 + 1.17x$	0.988	1.064–3.151
5d	3.102	$y = -0.66 + 1.35x$	0.964	2.002–4.268
5e	3.646	$y = -0.85 + 1.51x$	0.964	2.552–4.815
5f	3.996	$y = -0.96 + 1.60x$	0.959	2.900–5.178
5g	3.780	$y = -0.93 + 1.60x$	0.969	2.715–4.92
5h	3.521	$y = -0.81 + 1.48x$	0.960	2.425–4.689
5i	3.816	$y = -0.93 + 1.59x$	0.939	2.746–4.972
5j	2.128	$y = -0.55 + 1.55x$	0.907	0.574–3.886
5k	2.340	$y = -0.58 + 1.51x$	0.954	1.421–3.303
5l	2.273	$y = -0.59 + 1.55x$	0.943	1.379–3.210
5m	1.528	$y = -0.60 + 2.17x$	0.881	0.917–2.159
5n	1.805	$y = -0.33 + 1.37x$	0.960	1.009–2.645
5o	1.724	$y = -0.32 + 1.36x$	0.994	0.928–2.572
5p	2.571	$y = -0.47 + 1.18x$	0.941	1.455–3.759
5q	2.700	$y = -0.53 + 1.23x$	0.992	1.578–3.891
5r	2.681	$y = -0.51 + 1.20x$	0.988	1.537–3.898
5s	3.009	$y = -0.54 + 1.12x$	0.962	1.671–4.452
5t	3.995	$y = -0.69 + 1.16x$	0.959	2.442–5.714
Fluconazole	1.441	$y = -0.50 + 1.96x$	0.868	0.804–2.112
Epoxiconazole	0.815	$y = 0.24 + 1.64x$	0.946	0.107–1.704
Propiconazole	1.173	$y = 0.04 + 1.44x$	0.970	0.158–2.388

Note: EC_{50}, half maximal effective concentration; CL, confidence limit.

squares (PLS) regression. Leave-one-out cross-validation was performed on the training set compounds, and the composition score was modified to the optimal value obtained from cross-validation. Subsequently, comparative molecular field analysis (CoMFA) and comparative molecular similarity indices analysis (CoMSIA) models were established. Finally, the established models were utilized to predict the biological activity of compounds in the test set.

3 RESULTS AND DISCUSSION

3.1 Preparation of acrylopimaric acid triazole derivatives

In this study, acrylopimaric acid chloride and thiosemicarbazide were used as starting materials to synthesize acrylopimaric acid triazole using pyridine and sodium carbonate as solvents and acid-binding agents. The target compound was obtained by reacting acrylopimaric acid triazole with benzyl chloride, and their proton (^1H) nuclear magnetic resonance (NMR), carbon-13 (^{13}C) NMR, and liquid chromatography–mass spectrometry (LC–MS) spectral data can be found in the Supporting Information (Data S1 and S2, Figs S1–S90). Through observation of the reaction process, we found that the pH value during the acidification process has a certain influence on the yield of acrylopimaric acid triazole. When the pH is too high or too low, the yield decreases. Additionally, the reaction temperature also has a significant impact on the reaction. Too low a temperature leads to an incomplete reaction, while too high a temperature result in a complex reaction system with increased by-products. The optimal yield of the target compound is achieved under the most suitable reaction conditions.

3.2 Antifungal activity *in vitro*

The two series of synthesized compounds (**4a**–**4j** and **5a**–**5t**) were tested against six agricultural fungi. However, the results showed that both series of compounds exhibited low inhibitory activity against *C. orbiculare*, *F. graminearum*, *B. cinerea*, *S. sclerotiorum*, and *M. oryzae*, with the highest inhibition rate reaching only approximately 30% at a concentration of 50 mg/L (Supporting Information Table S1). However, these compounds demonstrate a certain inhibitory effect on *R. solani* (Table 1 and Fig. 1(a)). When both the thiol group and amino group were substituted with a benzyl group on the structure of acrylopimaric acid triazole, the

 © 2024 Society of Chemical Industry.

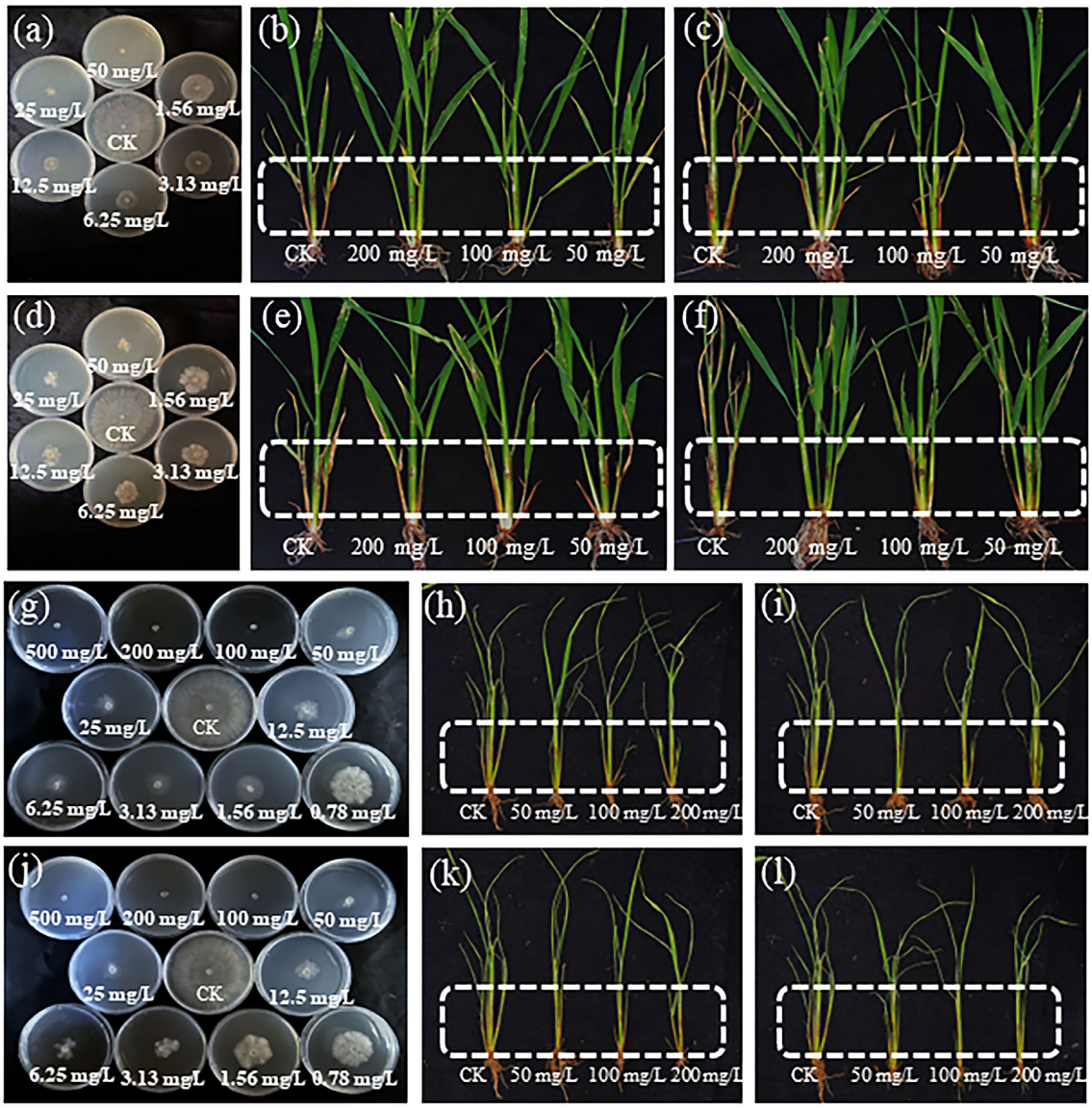


Figure 1. (a, d, g, j) *In vitro* antifungal activity of compound **5m**, fluconazole, epoxiconazole and propiconazole; (b, e, h, k) curative efficacy *in vivo* of compound **5m**, fluconazole, epoxiconazole and propiconazole on leaf sheaths and leaves; (c, f, i, l) protective efficacy *in vivo* of compound **5m**, fluconazole, epoxiconazole and propiconazole on leaf sheaths and leaves (200, 100, and 50 mg/L). CK, control.

compounds exhibited better activity compared to compounds with only a thiol group substitution. When the ortho position of the benzyl group was substituted with a nitro group, the inhibitory activity of the compounds reached its optimum state, with an inhibition rate still exceeding 50% even at 1.5625 mg/L. These results support the increased activity of the compounds in the presence of strong electron-withdrawing groups (–NO_2). This may be attributed to the electron-inductive effect of nitrogen in the nitro group on the carbon of the benzene ring, as the nitro group on the π orbital can form a conjugated π-π system with the delocalized π orbitals of the benzene ring, resulting in the coexistence of strong electron-inductive and electron-withdrawing conjugation effects. This leads to a significant decrease in electron cloud density in the benzene ring, accelerating intramolecular electron transfer and enhancing the antifungal activity of the compounds.

3.3 Antifungal activity *in vivo*

The protective efficacy (PE) and curative efficacy (CE) of compound **5m** against *R. solani* were determined through pot experiments. The results demonstrated that compound **5m** exhibited good protective and curative activities against *R. solani*, with a higher curative activity than protective activity. At concentrations of 200, 100, and 50 mg/L, compound **5m** showed PE values of 76.00%, 55.55%, and 36.00%, respectively, in rice leaf samples infected with *R. solani*; the corresponding CE values were 82.61%, 65.22%, and 47.83%, respectively. The protective activity of compound **5m** is superior to the PE of fluconazole, epoxiconazole, and propiconazole. Its CE is only superior to fluconazole but approaches that of epoxiconazole and propiconazole. (Figure 1(b),(c),(e),(f),(h),(i),(k),(l) and Tables S2 and S3).

 © 2024 Society of Chemical Industry.

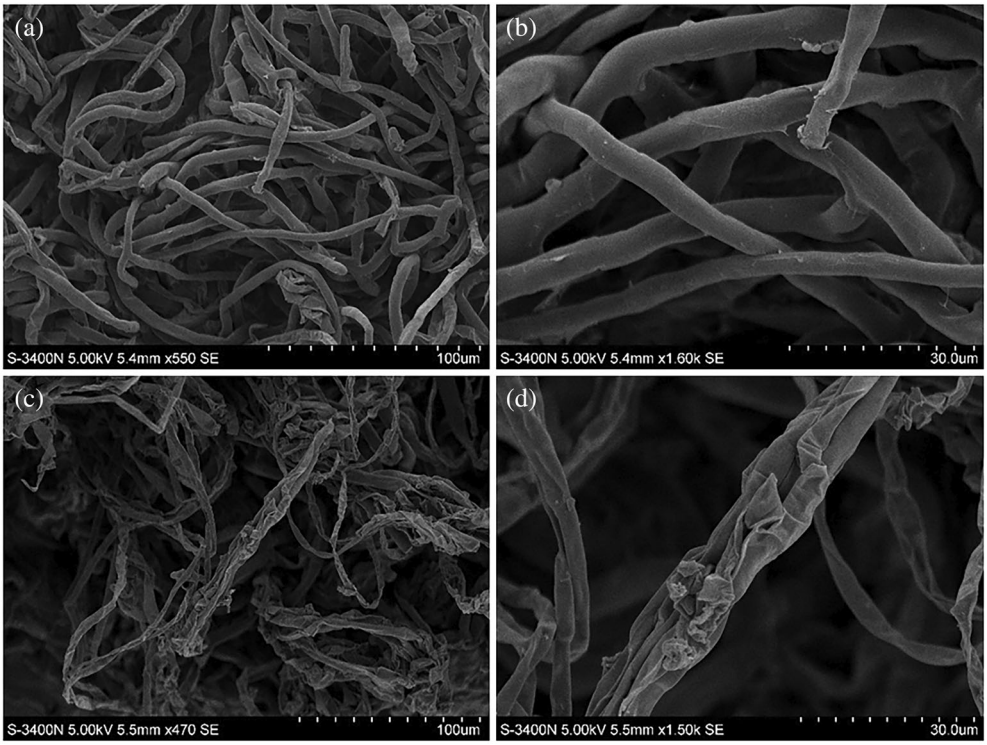


Figure 2. Effect of compound **5m** on mycelial morphology of *Rhizoctonia solani*. (a, b) Untreated plates; (c, d) plates treated with compound **5m** (1.528 mg/L). Scale bars represent 100 and 30 μm.

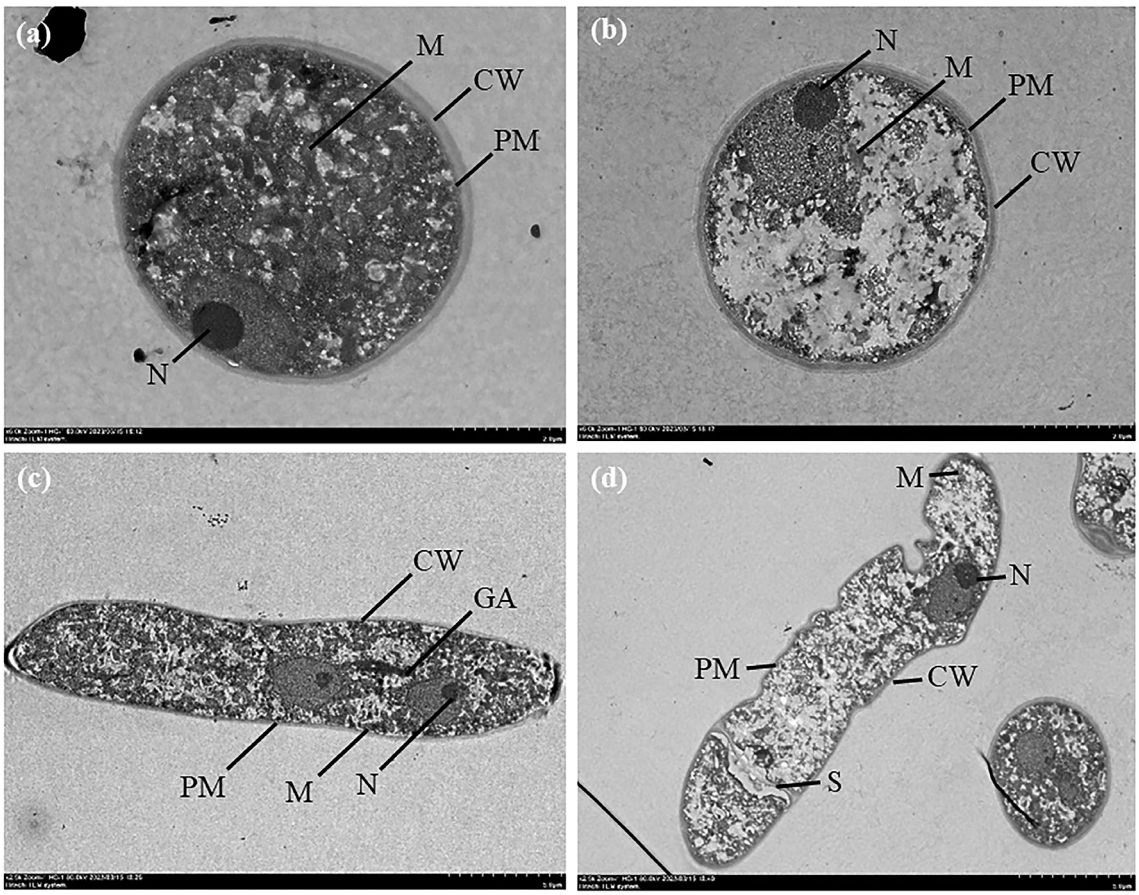


Figure 3. Effect of compound **5m** on the mycelial ultrastructure of *Rhizoctonia solani*. (a, c) Untreated plates; (b, d) plates treated with compound **5m** (1.528 mg/L). Scale bars represent 2 and 5 μm. CW, cell wall; S, septum; N, nuclei; M, mitochondria; PM, plasma membrane; GA, Golgi apparatus.

 © 2024 Society of Chemical Industry.

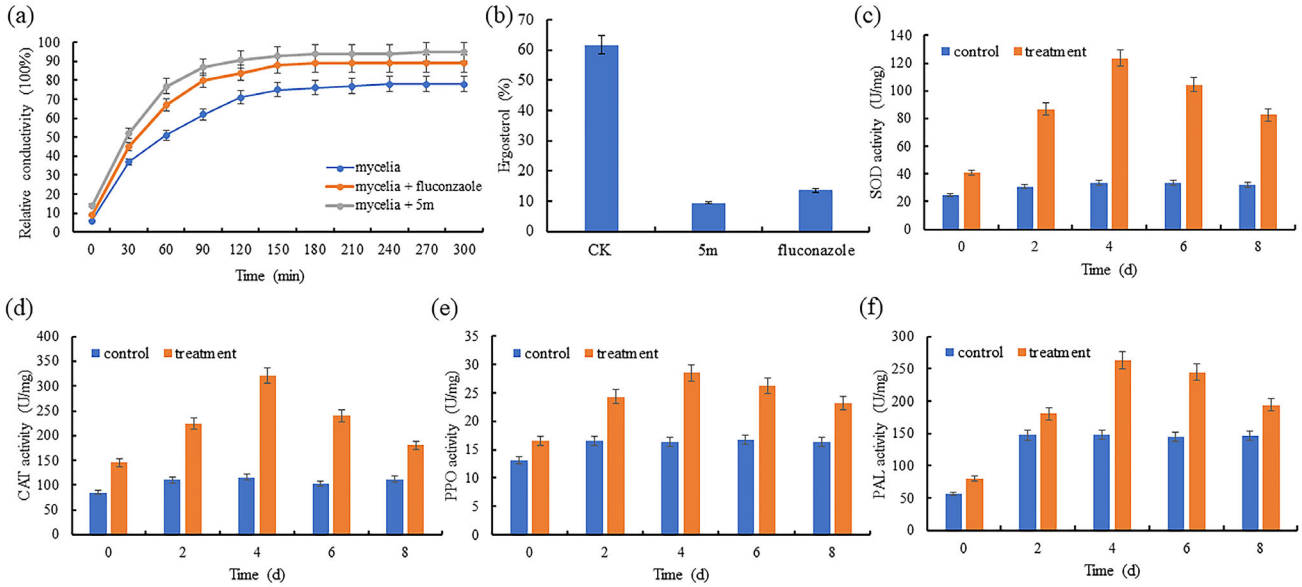


Figure 4. (a) The conductivity of mycelium treated with compound **5m** and control; (b) the ergosterol content after treatment with compound **5m** and control; (c–f) the SOD, CAT, PPO, and PAL activities of rice leaves treated with compound **5m**.

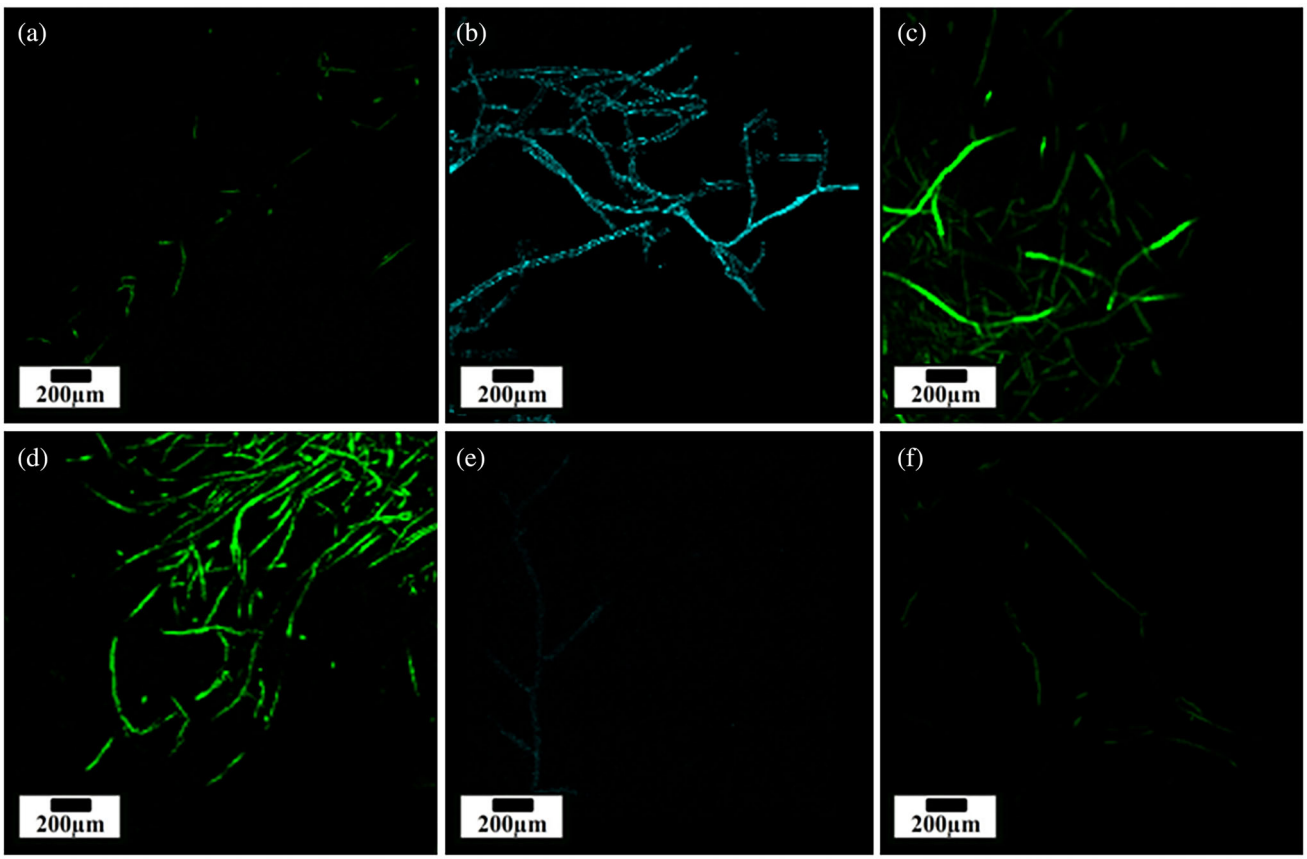


Figure 5. The staining results of mycelium. (a–c) Untreated plates; (d–f) plates treated with compound **5m** (1.528 mg/L). Scale bars represent 200 μm.

3.4 *Rhizoctonia solani* mycelial morphology and ultrastructure analysis

In the untreated group, the *R. solani* mycelium exhibited good growth, normal appearance, and a smooth and uniform surface. In the treatment group, severe wrinkling and collapse were observed on the surface of the mycelium, and the thickness was uneven (Fig. 2). In the control group, the organelles in the mycelial cells were clearly visible, with regularly shaped nuclei, intact

 © 2024 Society of Chemical Industry.

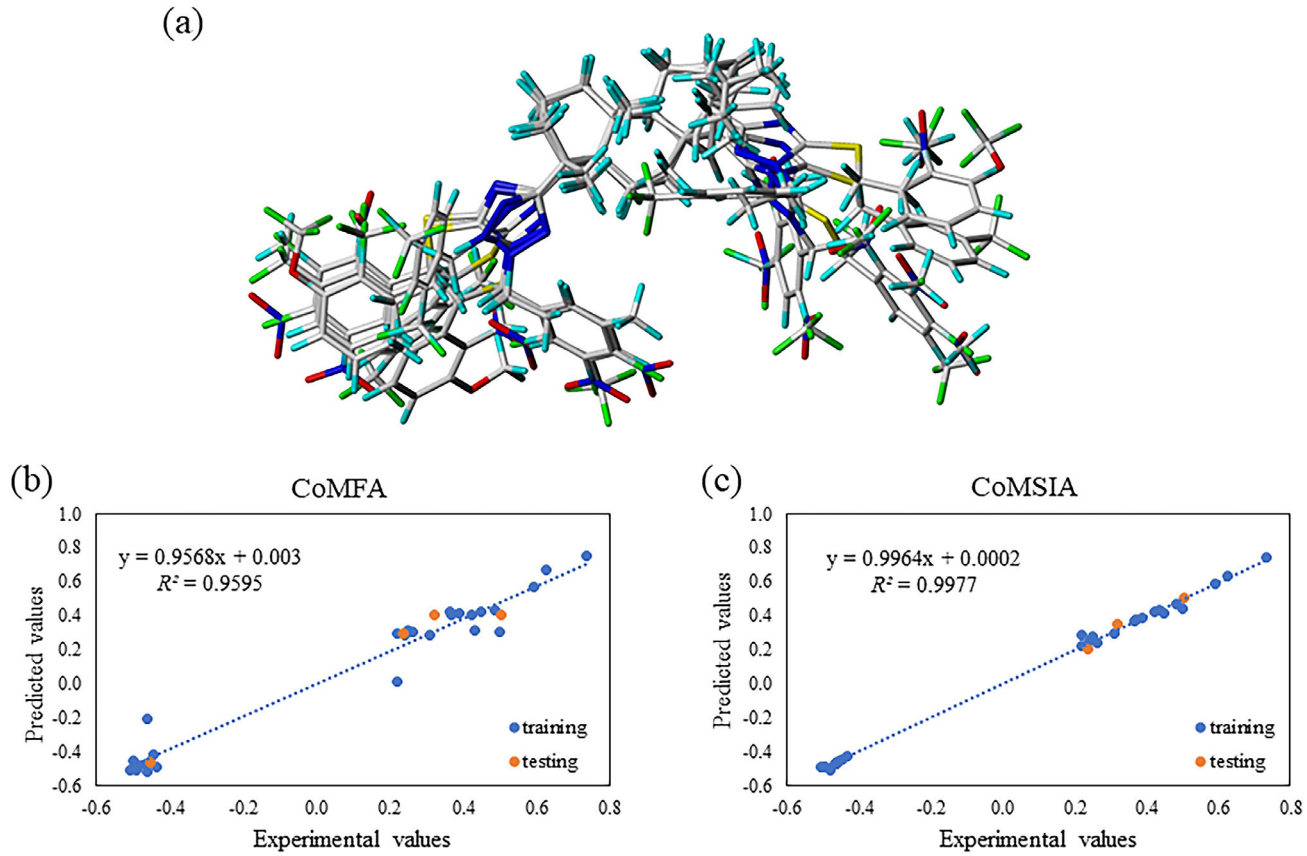


Figure 6. (a) Molecular alignment of the target compounds; (b, c) regression analysis of correlation between experimental values and predicted values.

mitochondria, and well-defined cell walls. In the treatment group, the ultrastructure of the mycelial cells was damaged, with deformed nuclei, irregular mitochondria, and cell membrane separation at the cell septum. Leakage of cell contents, vacuoles, and cytoplasm dissolution can be observed in the interior of the mycelium (Fig. 3).

3.5 *Rhizoctonia solani* mycelial cell membrane permeability analysis

Compared to the *R. solani* mycelium that were not treated with compound **5m**, the conductivity of the mycelium significantly increased after treatment with compound **5m**, indicating electrolyte leakage from the mycelium cells. The conductivity increased with time, with the highest rate of increase observed at 60 min. These results indicate that compound **5m** leads to an increase in cell membrane permeability (Fig. 4(a)).

3.6 Analysis of the effect on ROS production, nuclear morphology, and MMP of *R. solani*

2′,7′-Dichlorofluorescein diacetate (DCFH-DA), as a ROS indicator, can reflect the impact of different treatments on cellular ROS levels. As shown in Fig. 5(a),(d), compared to the mycelium in the untreated group, significant fluorescence appeared within the mycelium treated with compound **5m**, indicating the induction and accumulation of ROS by compound **5m**, which can lead to membrane permeabilization, cell damage, and even apoptosis. Hoechst 33258, as a nuclear fluorescence indicator, can reflect the effects of different treatments on the cell nucleus. As shown in Fig. 5(b),(e), compared to the control group, the mycelium treated with compound **5m** showed no significant blue fluorescence in the cell nucleus, and the discrete signals were weaker. Rhodamine 123, as a fluorescence indicator for mitochondria, can reflect the effects of different treatments on Mitochondrial Membrane Potential (MMP). As shown in Fig. 5(c),(f), compared to the control group, the fluorescence intensity within the mycelium treated with compound **5m** was significantly reduced, indicating that compound **5m** can disrupt MMP and impair mitochondria, leading to impaired mitochondrial function and accelerated cell apoptosis.

3.7 Analysis of the effect of compound 5m on the synthesis of ergosterol in *R. solani*

Ergosterol is a major component of cell membranes and directly influences membrane fluidity. Compared to untreated mycelium, treatment with compound **5m** resulted in a significant decrease in the ergosterol content within the mycelium. This suggests that Compound **5m** can inhibit the synthesis of ergosterol or promote its efflux (Fig. 4(b)).

3.8 Analysis of the effect of compound 5m on defense enzyme induction activity

To determine if the rice defense system was activated, we assessed the impact on four defense enzymes during rice leaf infection (Fig. 4(c)–(f)). We observed that the activity of all four defense enzymes was higher in the leaves treated with compound **5m** compared to the untreated control group. Throughout the 8-day experimental period, the activity of these defense

 © 2024 Society of Chemical Industry.

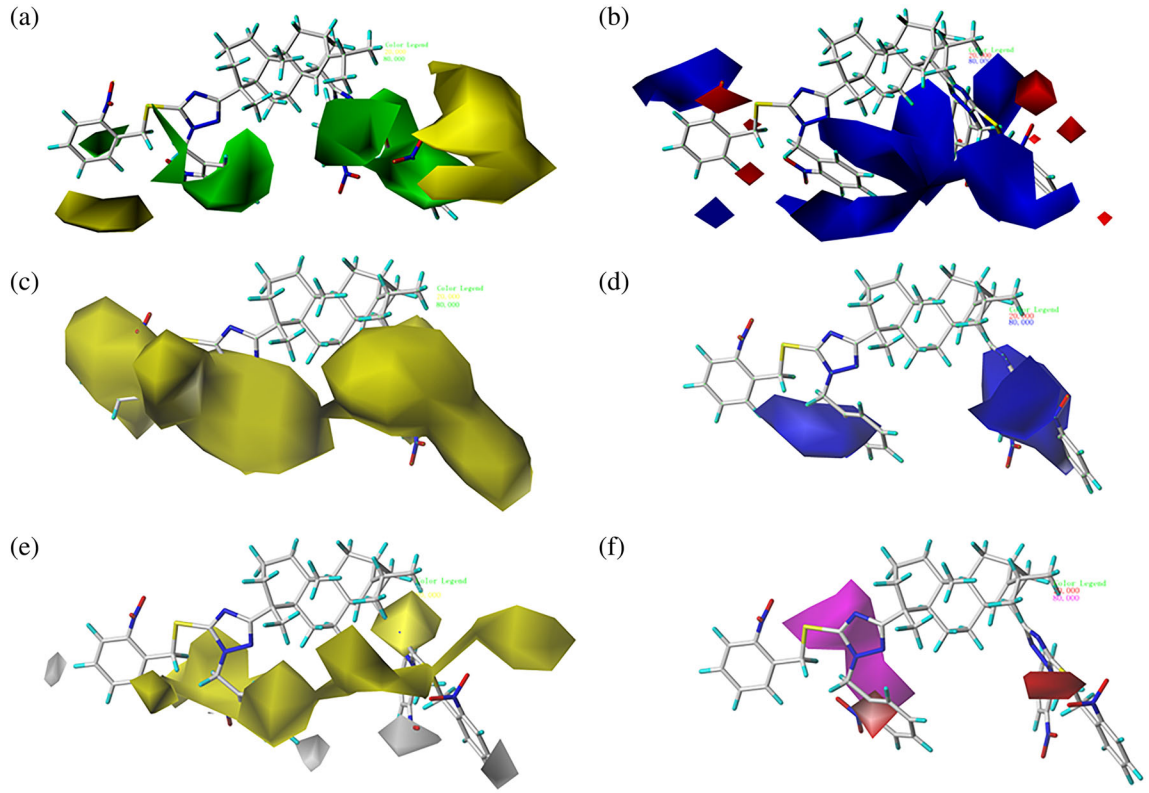


Figure 7. (a, b) Equipotential diagram of the CoMFA model for compound **5m**; (c–f) equipotential diagram of the CoMSIA model for compound **5m**.

enzymes initially increased and then decreased. On the fouth day, the SOD, CAT, PAL, and PPO activities reached their peaks, showing 3.68-, 2.76-, 1.74-, and 1.78-fold increases, respectively, compared to the untreated control. These results indicate that the presence of compound **5m** enhances the activity of defense enzymes in rice, thereby contributing to enhanced resistance in rice plants.

3.9 Three-dimensional quantitative structure–activity relationship (3D-QSAR) analysis

To further elucidate the relationship between the structure of acrylopimaric acid triazole derivatives and their antifungal activity, a 3D-QSAR model was established using compound **5m** as a template. The overlay of the compounds is shown in Fig. 6(a). The correlation coefficient and cross-validated coefficient of the model align with the recommended statistical values ($r^2 > 0.8$, $q^2 > 0.5$), demonstrating good correlation and predictive ability (Table S4). The predicted biological activities of the training and test sets of compounds are shown in Table S5 and Fig. 6(b),(c), respectively.

In the CoMFA model, the steric and electrostatic contributions of compound **5m** to its antifungal activity are depicted in Fig. 7(a),(b). In the steric field (Fig. 7(a)), there is a green region near the benzylamine group, indicating that the introduction of groups with high steric hindrance in this region favorably influences the antifungal activity. This is consistent with the observation that compounds with only a benzylthio group exhibit lower activity than those with both a benzylthio and a benzylamine group. In the electrostatic field (Fig. 7(b)), there are partial red regions near the phenyl ring, suggesting that the introduction of negatively charged groups in this region can enhance the compound's activity. For example, the presence of strong electron-withdrawing groups (–NO_2) at the ortho position of the benzyl group in compound **5m** leads to higher activity.

In the CoMSIA model, the steric, electrostatic, hydrophobic, and hydrogen bond acceptor fields based on compound **5m** are shown in Fig. 7(c)–(f). The steric and electrostatic fields are consistent with the structural modification information provided by the CoMFA model (Fig. 7(c),(d)). In the hydrophobic field (Fig. 7(e)), the yellow region covers a significant portion of the compound's structural framework, indicating the crucial role of hydrophobic interactions in the activity of this compound class. The introduction of hydrophobic groups at the benzylamine and benzylthio positions can significantly enhance the antifungal activity. In the hydrogen bond acceptor field (Fig. 7(f)), the red regions indicate that increasing the hydrogen bond acceptor field is beneficial for improving the activity, while the purple regions suggest the opposite. The red region is distributed near the nitro group connected to the benzylamine, indicating that the introduction of a group with hydrogen bond acceptor properties at this position would be beneficial for enhancing the activity. Overall, the 3D-QSAR model can provide valuable insights for the future optimization of acrylopimaric acid triazole derivatives as novel antifungal agents.

4 CONCLUSION

In this study, we designed and synthesized two series of acrylopimaric acid triazole derivatives (**4a**–**4j** and **5a**–**5t**), and the antifungal activities of the derivatives against *C. orbiculare*, *F. graminearum*, *B. cinerea*, *S. sclerotiorum*, *M. oryzae*, and *R. solani* were evaluated. The results showed that the acrylopimaric acid triazole derivatives containing both benzylamine and

 © 2024 Society of Chemical Industry.

benzylthio groups (**5a**–**5t**) exhibited better inhibitory effects against *R. solani* compared to derivatives without the benzylamine structure (**4a**–**4j**). Among these compounds, **5m** showed the best activity. Preliminary mechanistic studies indicated that compound **5m** could disrupt mycelial morphology, disrupt cell membrane permeability, decrease the ergosterol content, increase defense enzyme activity, induce the production and accumulation of ROS in cells, and impair mitochondrial function, leading to cell apoptosis. The 3D-QSAR analysis demonstrated that the antifungal activity of compound **5m** was influenced by its structural and charge distribution. This study aims to alleviate the pressure to use chemical fungicides and provide new fungicidal options for the control of *R. solani*.

ACKNOWLEDGEMENTS

The authors thank the National Natural Science Foundation of China (nos 31870555 and 32271810) for financial support.

CONFLICT OF INTEREST STATEMENT

The authors declare that there are no conflicts of interest.

DATA AVAILABILITY STATEMENT

The data that supports the findings of this study are available in the supplementary material of this article.

SUPPORTING INFORMATION

Supporting information may be found in the online version of this article.

REFERENCES

1 Pooja S, Purabi M, Ann HJ and Subramanian B, Sheath blight of rice: a review and identification of priorities for future research. *Planta* **250**: 1387–1407 (2019).
2 Wang C, Pi L, Jiang S, Yang M, Shu C and Zhou E, ROS and trehalose regulate sclerotial development in *Rhizoctonia solani* AG-1 IA. *Fungal Bio* **122**:322–332 (2018).
3 Hu WJ, Pan XL, Abbas HMK, Li FF and Dong WB, Metabolites contributing to *Rhizoctonia solani* AG-1-IA maturation and sclerotial differentiation revealed by UPLC-QTOF-MS metabolomics. *PloS One* **12**:1–16 (2017).
4 Ajayi-Oyetunde OO and Bradley CA, *Rhizoctonia solani*: taxonomy, population biology and management of rhizoctonia seedling disease of soybean. *Plant Pathol* **67**:3–17 (2018).
5 Zheng A, Lin R, Zhang D, Qin P, Xu L, Ai P *et al.*, The evolution and pathogenic mechanisms of the rice sheath blight pathogen. *Nat Commun* **4**:1424–1723 (2013).
6 Joana BA, Michelangelo S, Marcello Z, Wang WX, Jiang DH, Li SD *et al.*, Genetic structure of populations of the rice infecting pathogen *rhizoctonia solani* AG-1 IA from China. *Phytopathology* **99**:1090–1099 (2009).
7 Zhao YT, Wang XG, Zhang L, Wang KY, Wu YC, Yao J *et al.*, Anti-fungal activity of *Moutan cortex* extracts against Rice sheath blight (*rhizoctonia solani*) and its action on the pathogen's cell membrane. *ACS Omega* **7**:47048–47055 (2022).
8 Yao TT, Xiao DX, Li ZS, Cheng JL, Fang SW, Du YJ *et al.*, Design, synthesis, and fungicidal evaluation of novel pyrazole-furanand pyrazole-pyrrole carboxamide as succinate dehydrogenase inhibitors. *J Agric Food Chem* **65**:5397–5403 (2017).
9 Zhao SY, Lin GS, Duan WG, Zhang QA, Huang YL and Lei FH, Design, synthesis, and antifungal activity of novel longifolene-derived diacylhydrazine compounds. *ACS Omega* **6**:9104–9111 (2021).
10 Paulo S, Chantal F, Lillian B, Isabel CFRF, Leonel P and Teresa G, The antifungal activity of extracts of *Osmundea pinnatifida*, an edible seaweed, indicates its usage as a safe environmental fungicide or as a food additive preventing post-harvest fungal food contamination. *Food Funct* **9**:6187–6195 (2018).
11 Bento TS, Torres LMB, Fialho MB and Bononi VLR, Growth inhibition and antioxidative response of wood decay fungi exposed to plant extracts of *Casearia* species. *Lett Appl Microbiol* **58**:79–86 (2014).
12 Yi H, Chen Y, Liu J, Zhang J, Guo W, Xiao W *et al.*, Extraction and separation of active ingredients in *Schisandra chinensis* (Turcz.) Baill and the study of their antifungal effects. *PloS One* **11**:1–22 (2017).
13 Tao P, Wu CY, Hao J, Gao YQ, He XH, Li J *et al.*, Antifungal application of rosin derivatives from renewable pine resin in crop protection. *J Agric Food Chem* **68**:4144–4154 (2020).
14 Mao SY, Wu CY, Gao YQ, Hao J, He XH, Tao P *et al.*, Pine rosin as a valuable natural resource in the synthesis of fungicide candidates for controlling *fusarium oxysporum* on cucumber. *J Agric Food Chem* **69**:6475–6484 (2021).
15 Yadav BK, Gidwani B and Vyas A, Rosin: recent advances and potential applications in novel drug delivery system. *J Bioact Compat Pol* **31**: 111–126 (2016).
16 Kulabaş N, Tatar E, Özakpınar ÖB, Özsavcı D, Pannecouque C, Clercq ED *et al.*, Synthesis and antiproliferative evaluation of novel 2-(4H-1,-2,4-triazole-3-ylthio) acetamide derivatives as inducers of apoptosis in cancer cells. *Eur J Med Chem* **121**:58–70 (2016).
17 Cui P, Li X, Zhu M, Wang B, Liu J and Chen H, Design, synthesis and antimicrobial activities of thiouracil derivatives containing triazolothiadiazole as SecA inhibitors. *Eur J Med Chem* **127**:159–165 (2017).
18 Isloor AM, Kalluraya B and Shetty P, Regioselective reaction: synthesis, characterization and pharmacological studies of some new Mannich bases derived from 1,2,4-triazoles. *Eur J Med Chem* **44**:3784–3787 (2009).
19 Küçükgüzel I, Küçükgüzel SG, Rollas S and Kiraz M, Some 3-Thioxo/alkylthio-1,2,4-triazoles with a substituted thiourea moiety as possible antimycobacterials. *Bioorg Med Chem Lett* **11**:1703–1707 (2001).
20 Fan ZJ, Shi J and Bao XP, Synthesis and antimicrobial evaluation of novel 1,2,4- triazole thioether derivatives bearing a quinazoline moiety. *Mol Divers* **22**:657–667 (2018).
21 Gao Y, Li L, Chen H, Li J, Song Z, Shang S *et al.*, High value-added application of rosin as a potential renewable source for the synthesis of acrylopimaric acid-based botanical herbicides. *Ind Crops Prod* **78**: 131–140 (2015).

 © 2024 Society of Chemical Industry.